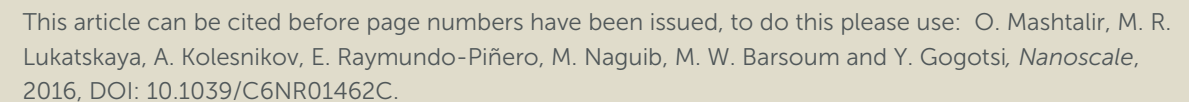
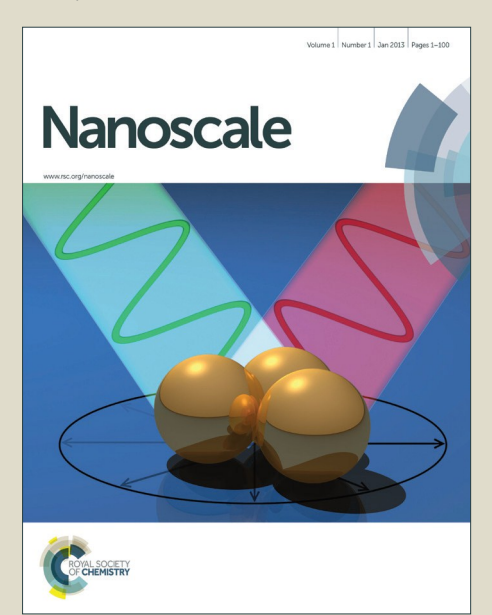


Nanoscale

Accepted Manuscript





This is an *Accepted Manuscript*, which has been through the Royal Society of Chemistry peer review process and has been accepted for publication.

Accepted Manuscripts are published online shortly after acceptance, before technical editing, formatting and proof reading. Using this free service, authors can make their results available to the community, in citable form, before we publish the edited article. We will replace this Accepted Manuscript with the edited and formatted Advance Article as soon as it is available.

You can find more information about *Accepted Manuscripts* in the **Information for Authors**.

Please note that technical editing may introduce minor changes to the text and/or graphics, which may alter content. The journal's standard <u>Terms & Conditions</u> and the <u>Ethical guidelines</u> still apply. In no event shall the Royal Society of Chemistry be held responsible for any errors or omissions in this *Accepted Manuscript* or any consequences arising from the use of any information it contains





Nanoscale

COMMUNICATION

Effect of hydrazine intercalation on structure and capacitance of 2D titanium carbide (MXene)†

Received 00th January 20xx, Accepted 00th January 20xx

DOI: 10.1039/x0xx00000x

O. Mashtalir,‡§^a M. R. Lukatskaya,‡^a A. I. Kolesnikov,^b E. Raymundo-Piñero,^c M. Naguib,^d M.W. Barsoum,^a and Y. Gogotsi ^{a*}

www.rsc.org/

Published on 25 March 2016. Downloaded by Drexel University on 25/03/2016 10:26:56.

Herein we show that hydrazine intercalation into 2D titanium carbide (MXene) results in changes in materials surface chemistry by decreasing the amount of OH surface groups and intercalated water. It also creates a pillaring effect between ${\rm Ti}_3 {\rm C}_2 {\rm T}_x$ layers preopening the structure and improving accessability to active sites. The hydrazine treated material has demonstrated a greatly improved capacitance of 250 F/g in acidic electrolyte with an excellent cycling ability for electrodes as thick as 75 μm .

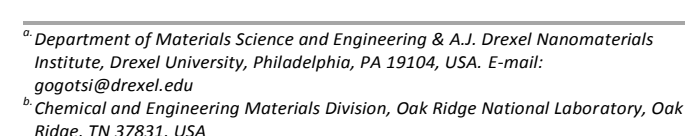
Since the discovery of graphene, there has been a great interest in novel two-dimensional (2D) materials owing to their high surface areas and properties that differ from their 3D analogues. Among these materials, MXenes, a recently discovered family of 2D transition metal carbides and carbonitrides, are receiving increasing attention. Produced by the selective etching of "A" element layers (mostly Al) from the MAX phases, they consist of the $M_{n+1}X_n$ layers, where M is an early transition metal, X is carbon and/or nitrogen, n=1,2 or 3. MXenes exhibit a unique combination of various properties, including, but not limited to, metallic conductivity and hydrophilicity, that make them quite attractive for energy storage applications.

To date, MXenes have shown promising performance as active electrode materials in electrochemical capacitors.⁶⁻⁸ It was also established that similar to other 2D materials, their energy storage properties can be enhanced in various ways. As in the case of graphene, which usually shows moderate performance due to restacking,⁹ the area of electrochemically active surface can be increased *via* the introduction of defects

by potassium hydroxide (KOH) activation,¹⁰ sheet pillaring by intercalation of molecules,^{11, 12} porosity development ("holey" graphene),^{13, 14} etc.

Similarly, MXenes have been modified by separating their multilayer stacks into monolayer sheets. Assembled by filtration of delaminated Ti₃C₂T_x solutions, 5-20 μm thick "paper" electrodes – binder/additive free^{6, 7} and composites^{15,} ¹⁶ – which showed volumetric capacitances, that were much higher than those of conventional carbon materials. However, while such "dimensions" are perfectly suited for microsupercapacitors, there are other energy storage devices that require much higher loadings of the material and, consequently, thicker electrodes. ¹⁷ To fulfil this need, chemical modification of the multilayer Ti₃C₂T_x - where T is a surface termination, usually OH and F, that replaces the etched Allayers - in basic aqueous solutions, such as KOH, was proposed in order to produce predominantly oxygen terminated MXene surfaces which offer better performance compared to nonmodified ones. 18 It has been shown that many polar organic molecules and positively charged ions can spontaneously intercalate MXenes, affecting their interlayer spacing, surface chemistry and properties. 19-21

In this study we investigated the effect of intercalation of one of those molecules, hydrazine monohydrate, HM $(N_2H_4*H_2O)$, on the $Ti_3C_2T_x$ surface chemistry and, subsequently, the electrochemical performance of the latter in



CNRS, CEMHTI UPR3079, Univ. Orléans, F-4071 Orléans, France

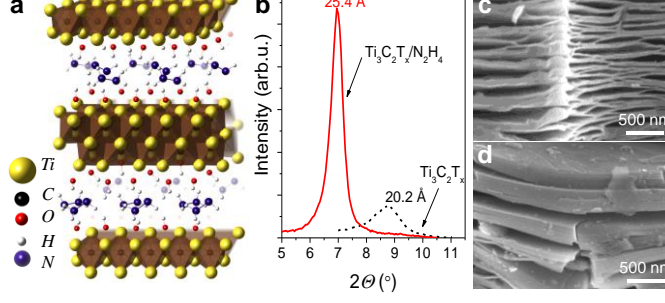


Fig. 1. (a) Structural model of $Ti_3C_2OH + 0.5N_2H_4$. (b) X-Ray diffraction patterns around the $Ti_3C_2T_x$ (0002) peak before, and after, hydrazine treatment; the numbers show the corresponding *c*-lattice parameter values. (c, d) SEM images of $Ti_3C_2T_x$ particles before and after hydrazine intercalation, respectively (same scale).

This journal is © The Royal Society of Chemistry 20xx

Nanoscale, 2016, **00**, 1-5 | **1**

^{d.} Materials Science and Technology Division, Oak Ridge National Laboratory, Oak Ridge, TN 37831

[†] Electronic Supplementary Information (ESI) available: Characterization methods, additional XRD patterns (Fig. S1) and INS spectra (Figs. S2-S4). See DOI: 10.1039/x0xx00000x

[‡] These authors contributed equally to this work.

[§] Current address: Department of Chemistry, Research Foundation at the City University of New York, New York, NY 10031, USA.

COMMUNICATION Nanoscale

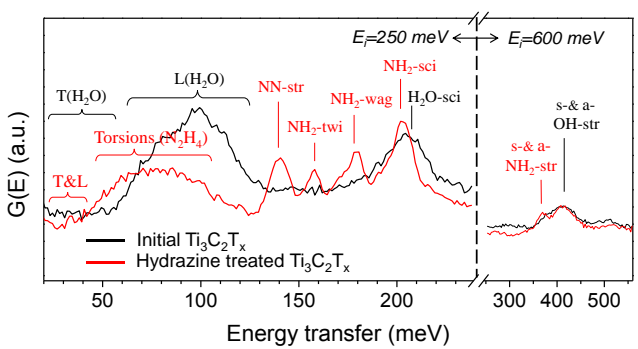


Fig. 2. Inelastic neutron scattering spectra for $Ti_3C_2T_x$ before (black curve) and after (red curve) hydrazine treatment measured with different E_i , 250 and 600 meV, at 7 K. T and L stand for translational and librational modes.

various electrolytes.

Published on 25 March 2016. Downloaded by Drexel University on 25/03/2016 10:26:56.

A schematic illustration of the Ti₃C₂T_x layered structure intercalated with HM molecules is shown in Fig. 1a. The primary evidence for intercalation is the shift of the main (0002) Ti₃C₂T_x XRD peak toward lower 20 angles after treatment in a HM aqueous solution (Fig. 1b; see also Supporting Fig. S1 †). This shift corresponds to c lattice parameter (c-LP) increase from 20.2 Å to 25.4 Å, suggesting the formation of a nearly complete monolayer of N₂H₄ molecules in the space between the Ti₃C₂T_x layers.¹⁹ Furthermore, the (0002) peak intensity increases after intercalation signifying that the intercalated structure is better organized – at least along the c-axis. SEM images collected for material before and after HM treatment (Fig. 1c and d, respectively) show the formation of ~ 100 nm-thick lamellas of Ti₃C₂T_x layers apparently glued together by the intercalant. Based on the Scherer formula, the average crystalline size along c direction calculated from the XRD patterns in Fig. 1b is 20.4 nm.

To gain insight into the chemical changes at the Ti₃C₂T_x surface upon HM treatment, highly hydrogen atoms sensitive inelastic neutron scattering, INS, analysis was performed on the MXene powders before, and after, intercalation. In Fig. 2, the INS spectrum for the initial Ti₃C₂T_x (black curve) powders reveals the presence of water and hydroxyl groups in the sample, evidenced by a broad intermolecular librational band of bound water, that extends from 50 to 120 meV, intramolecular H-O-H scissors mode of un-dissociated H₂O, centered at ~205 meV, and a broad band of superimposed O-H stretching modes in the 350-460 meV range, with a maximum at ~415 meV. 22, 23 The latter is a combination of symmetric and asymmetric O-H stretching vibrations coming from water molecules (typically within the 390-430 meV range) and surface-bound hydroxyl groups at ~450 meV, as reported for hydrated anatase²² and kaolinite²⁴. The extension of stretching modes down to 350 meV implies the formation of strong O···H-O hydrogen bond networks which causes weakening of the O-H covalent bonds of the water molecule. In addition, broad distribution of the translational (below 40 meV) and librational bands (50-120 meV) and the absence of distinct peaks within these regions (in particular, no acoustic peak of ice at ~7 meV; see Supporting Fig. S2†) suggest that strong hydrogen bonding

occurs between the H_2O and OH-terminated Ti_3 CaTarsurface, rather than between water molecules the results have confirmed the presence of relatively strongly bonded H_2O molecules to OH terminations in $Ti_3C_2T_x$.

In contrast to the INS spectrum before intercalation, the intensity of the aforementioned H_2O/OH vibration modes is significantly reduced after HM treatment (red curve in Fig. 2). Thus, librational and bending modes of undissociated water as well as two bands of low intensity at ~300 and 500 meV – overtones due to combinations of the librational and bending and stretching modes, respectively, 27 – mostly vanished. The intensity of the OH stretching modes also greatly decreased. The difference in intensities suggests reduction of hydrogen content (as OH groups and H_2O) by a factor of 2.185 upon HM treatment; hence the final HM intercalated $Ti_3C_2T_x$ contains about 46% of the initial H.

Instead of H₂O/OH vibration modes, sharp peaks, indicative of hydrazine molecules' stretching and bending modes appeared. Those include a N-N stretching mode, strongly affected by hydrogen from N-H covalent bonding and located at 140 meV, NH₂ bending modes (rocking, twisting, waging and scissoring at 120, 158, 179, and 203 meV, respectively) and NH₂ stretching modes.^{28, 29} The latter is assigned to a sharp peak at 370 meV and a wide band stretched up to 470 meV (see also Supporting Fig. S3†). 24,29 Note that this region might be also affected by H₂O/OH stretches found in the sample before intercalation. Low-energy peaks (up to 100 meV) may be assigned to translational/librational (up to 40 meV) and torsional modes (40-110 meV) of hydrazine. The modes appear to be quite broad and no pronounced peaks are observed suggesting a high degree of disorder of N₂H₄ within the Ti₃C₂T_x layers, which is consistent with the presence of a monolayer of

Low packing density of hydrazine molecules between the layers hints that intercalant molecules would act as 'pillars' for $\text{Ti}_3\text{C}_2\text{T}_x$ layers without blocking access to electrochemically active sites. Thus, comparison of INS spectra of $\text{Ti}_3\text{C}_2\text{T}_x$ before, and after, HM treatment confirms HM intercalation and removal of a significant number of OH terminations and H_2O molecules.

The HM intercalation was also found to be reversible. Heating the multilayer flakes for 30 h in low vacuum at 150°C, resulted in the disappearance of the HM modes from the INS spectrum (Supporting Fig. S4†).

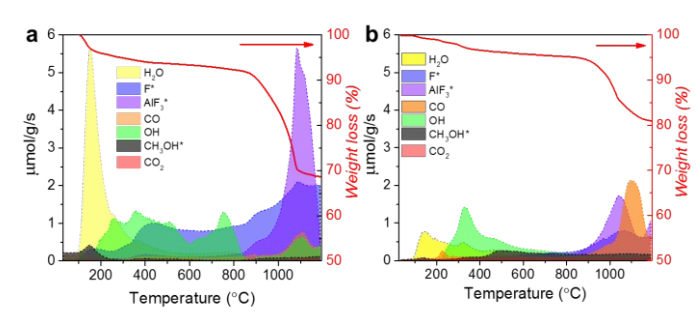


Fig. 3. Temperature programmed desorption mass spectroscopy data for $Ti_3C_2T_x$ (a) before and, (b) after hydrazine treatment. Species marked with asterisks were not quantified and are plotted in arbitrary units.

Published on 25 March 2016. Downloaded by Drexel University on 25/03/2016 10:26:56.

Nanoscale COMMUNICATION

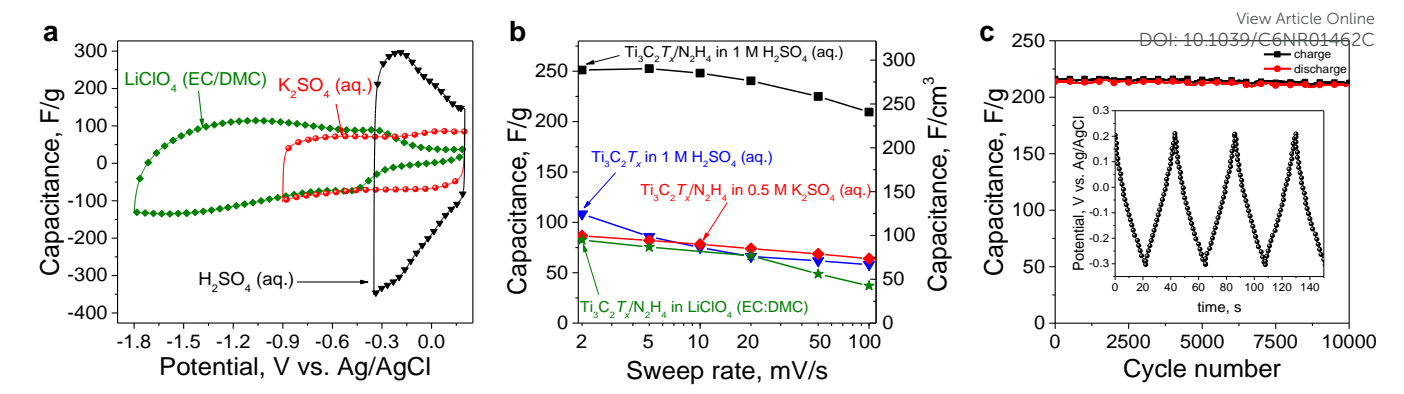


Fig. 4. Electrochemical performance of hydrazine treated $Ti_3C_2T_x$: (a) cyclic voltammetry data collected at 10 mV/s in aqueous 1 M H_2SO_4 (black triangles), 0.5 M H_2SO_4 (red circles) and non-aqueous 1 M H_2SO_4 in EC/DMC (green diamonds), (b) summary of rate performances extracted from CV data in different electrolytes and comparison with the performance of the untreated $Ti_3C_2T_x$ in H_2SO_4 electrolyte. In this figure the gravimetric capacitance is plotted on the left y-axis and the corresponding volumetric one on the right y-axis. (c) capacitance retention test for hydrazine-treated $Ti_3C_2T_x$ galvanostatically cycled at 5 A/g in 1 M H_2SO_4 . Inset illustrates galvanostatic data for few cycles.

In order to acquire complementary information about changes in Ti₃C₂T_x surface chemistry and thermal stability after hydrazine treatment, we performed temperature programmed desorption mass spectroscopy (TPD-MS). The spectrum recorded for pristine Ti₃C₂T_x powders (Fig. 3a) revealed two temperature regions where a substantial weight loss occurred. The first range between 100-200 °C is related to water evolution. It is followed by a period of thermal desorption of surface functional groups, such as OH, F and carbon oxides. The second weight loss range between 800-1200 °C corresponds to 2 processes: i) the irreversible transformations within the MXene structure due to disproportionation of MXene and formation of cubic TiC, TiO₂ and CO/CO₂ gas evolution, and ii) thermal decomposition of AIF₃·nH₂O³⁰ (AIF₃ is a by-product of the Ti₃AlC₂ HF etching step). Note, that the amount of desorbed AIF3 was not quantified due to the absence of a standard and is presented in the graph in arbitrary units (normalized by weight of the sample) and not µmol/g/s. The same is true for all entities that are marked with asterisks.

A comparison of the TPD MS data for pristine and HM intercalated ${\rm Ti_3C_2T_x}$ shown in Figs. 3a and b, respectively, shows a significant decrease in the intensity of the regions corresponding to ${\rm H_2O}$ and ${\rm AlF_3}$ species, suggesting their removal during the HM treatment: amounts of the ${\rm AlF_3}$ and ${\rm H_2O}$ released decreased by a factor of 4 (compare Fig. 3a and b). While removal of ${\rm AlF_3}$ can be due to washing it out upon HM treatment, ${\rm H_2O}$ is expected to be exchange with hydrazine molecules. In agreement with INS results, a comparison of Fig. 3a and b confirms that pristine ${\rm Ti_3C_2T_x}$ powders contained a larger amount of ${\rm H_2O}$ and OH groups than the hydrazine treated ones.

It is important to note that in case of the hydrazine treated ${\rm Ti_3C_2T_x}$ we were unable to distinguish contributions from the hydrazine and hydroxyl desorption, since both of them yield species with the same mass-to-charge ratio, m/z. Also, it is reasonable to assume that the increased amounts of CO evolved at higher temperatures for the hydrazine treated

 ${\rm Ti_3C_2T_x}$ can be attributed to the larger amounts of oxygencontaining functional groups vs. the F-containing ones. Thus, the observed increase in the temperature of the weight loss onset (restructuring and decomposition of MXene)^{31, 32} and a smaller total mass loss suggest that the stability of MXene improved as a result of HM intercalation (Fig. 3b).

We performed electrochemical characterization of the HM treated Ti₃C₂T_x in acidic and neutral aqueous electrolytes, viz. H₂SO₄ and K₂SO₄, respectively, as well as a standard Li-ion organic electrolyte, viz. 1 M LiClO₄ in ethylene carbonate/dimethyl carbonate, EC/DMC. Typical cyclic voltammetry profiles and rate performance in these electrolytes are shown in Figs. 4a and b, respectively. The highest specific capacitance and excellent capacitance retention at rates up to 100 mV/s were observed for the HM treated Ti₃C₂T_x in 1 M H₂SO₄, showing a ≈ 3 fold increase over untreated Ti₃C₂T_x (Fig. 4b), which can be explained by: changes in materials surface chemistry as a result of HM treatment, i.e. according to TPD-MS decreased number of electrochemically inactive Ti-F surface groups 18 is observed, since those are unstable in high pH solutions (similar to what was observed for KOH-treated $Ti_3C_2T_x^{18}$) and, ii) since the intercalant molecules cause the distance between MXene layers 19 to increase, it renders redox active³³ sites rapidly accessible to the protons.

The use of neutral K_2SO_4 electrolyte allowed us to increase the voltage window to 1.1 V. However, because the hydrated K^+ ion is significantly larger and slower than a proton, the resulting capacitances are lower (Fig. 4a and b) [which can be explained from geometry point of view when electrolytes with large cations such as K^+ are used instead of smallest H^+ ions a smaller number of active sites can participate in the energy storage process]. It is worth mentioning that hydrogen ion H^+ does not exist as a free species in condensed phases and H_3O^+ and $H_5O_2^+$ are usually responsible for fast transport of protons H_3^+ by Grotthuss proton hopping mechanism. In the case of hydrazine intercalation, hydrazinium H_2^+ and hydrazonium, H_2^+ ions may also be involved, H_3^+ but identification of exact ion transport and charge storage

oscale Accepted Manusc

COMMUNICATION Nanoscale

mechanisms will require a detailed spectroscopic study, which is outside the scope of this paper.

Further increase in voltage window (2 V) was achieved in non-aqueous solution of 1 M LiClO $_4$ in EC/DMC used a 1:1 volume ratio (Fig. 4a and b). It is worth noting that a combination of factors, such as electrolyte conductivity, solvent, etc., affects the energy storage. Therefore, performance in organic electrolytes should not be directly compared to performance in aqueous electrolytes, and while ${\rm Li}^+$ ion size is smaller than ${\rm K}^+$, the observed capacitance in EC/DMC is slightly lower than capacitance in ${\rm K}_2{\rm SO}_4$ (aq.). Yet, despite the lower values for the capacitances in EC/DMC, the energy density is higher than in the ${\rm H}_2{\rm SO}_4$ because of the larger voltage window.

Lastly, galvanostatic cycling data - collected at 5 A/g in 1 M H_2SO_4 - of HM treated $Ti_3C_2T_x$ demonstrate high gravimetric and volumetric capacitances of 215 F/g and 250 F/cm³, respectively; triangular profiles (inset Fig. 4c) - with almost no IR drop - and no capacitance degradation after 10,000 cycles (Fig. 4c).

Conclusions

Hydrazine intercalation into $Ti_3C_2T_x$, leads to a significant decrease in the water content and the amount of fluoride terminations. Moreover we observed high volumetric and gravimetric capacitances in a sulphuric acid electrolyte along with an excellent rate performance and cyclability of the hydrazine treated material. We attribute this to changes in surface chemistry as well as pillaring of the $Ti_3C_2T_x$ sheets by the intercalant molecules, which allows an easy access for protons and supports fast charge/discharge kinetics.

Experimental section

Powders of $Ti_3C_2T_x$ were synthesized by etching Ti_3AlC_2 MAX phase powders. The latter, with a particle size < 38 µm, was treated with 50% aqueous hydrofluoric, HF, solution (Fisher Scientific, Fair Lawn, NJ) at room temperature (RT), for 18 h. The resulting suspension was washed six to eight times, using deionized water, and separated from the remaining HF by centrifuging until the pH of the supernatant was \approx 6. The wet sediment was then divided into 2 portions of equal weight. The first portion was used for intercalation without drying. The second portion was filtered through a polypropylene membrane (3501 Coated PP, Celgard LLC, Charlotte, NC), washed with ethanol, and placed in a desiccator under vacuum (<10 Torr) at RT for drying and storage. This sample was used as a reference sample for XRD analysis (after 24 h of drying) and electrochemical study.

To intercalate ${\rm Ti_3C_2T_x}$ with HM, the wet ${\rm Ti_3C_2T_x}$ powder was suspended in HM (HM:MXene weight ratio of 10:1) and stirred for 24 h at RT. Later, the resulting colloidal solution of hydrazine treated powder was filtered and washed with ethanol. The powder was then dried and stored in a desiccator

under vacuum (<10 Torr) at RT for 24 h and then used for XRD analysis and electrode preparation.

DOI: 10.1039/C6NR01462C

Electrodes for the electrochemical study were prepared by rolling a pre-mixed slurry, containing ethanol (190 proof, Decon Laboratories, Inc.), $\text{Ti}_3\text{C}_2\text{T}_x$ powder (either pristine or HM treated), polytetrafluoroethynene (PTFE) binder (60 wt.% in H₂O, Aldrich) and carbon black, CB, which was added to create a conductive network in-between the particles. The resulting electrodes - were used for all electrochemical experiments - contained: 90 wt. % $\text{Ti}_3\text{C}_2\text{T}_x$, 5 wt. % carbon black, 5 wt. % PTFE and were 70 µm thick.

Activated carbon film electrodes were prepared following the same procedure described above for the $Ti_3C_2T_x$ electrodes, but without CB. The resulting activated carbon electrodes composition was 95 wt. % of YP-50 activated carbon (Kuraray, Japan) and 5 wt. % of the PTFE. The electrodes were 100-150 μm thick.

All electrochemical measurements were performed in 3-electrode Swagelok cells, where the pristine or HM treated ${\rm Ti_3C_2T_x}$ films served as working electrodes, the over-capacitive activated carbon was used as counter electrodes, and Ag/AgCl in 1 M KCl was used as a reference in order to precisely control electrochemical potentials.

Cyclic voltammetry, electrochemical impedance spectroscopy and galvanostatic cycling were performed using a VMP3 potentiostat (Biologic, Claix, France). Cyclic voltammetry was performed using scan rates from 1 mV/s to 100 mV/s. Galvanostatic cycling was performed at 0.1, 1 and 10 A/g.

Details on characterization techniques can be found in ESI file $^{\scriptsize +}$.

Acknowledgements

We thank Dr. Babak Anasori for providing Ti_3AlC_2 , Patrick Urbankowski for preparing $Ti_3C_2T_x$ and hydrazine treated $Ti_3C_2T_x$ samples for the second round of INS study, Prof. Patrice Simon for helpful discussions, and Prof. Vadym Mochalin for writing a proposal to obtain neutron scattering beam time at the Neutron Spallation Source. We thank the Centralized Research Facilities of Drexel University for providing access to XRD and SEM. VESTA software was used for visualization (Fig. 1a). This work was supported by the Fluid Interface Reactions, Structures and Transport (FIRST) Center, an Energy Frontier Research Center funded by the U.S. Department of Energy, Office of Science, Office of Basic Energy Sciences. The research at Oak Ridge National Laboratory's Spallation Neutron Source was sponsored by the Scientific User Facilities Division, Office of Basic Energy Sciences, U.S. Department of Energy.

Notes and references

 A. C. Ferrari, F. Bonaccorso, V. Fal'ko, K. S. Novoselov, S. Roche, P. Boggild, S. Borini, F. H. L. Koppens, V. Palermo, N. Pugno, J. A. Garrido, R. Sordan, A. Bianco, L. Ballerini, M. Prato, E. Lidorikis, J. Kivioja, C. Marinelli, T. Ryhanen, A. Morpurgo, J. N. Coleman, V. Nicolosi, L. Colombo, A. Fert, M. Garcia-Hernandez, A. Bachtold, G. F. Schneider, F. Guinea, C. Dekker, M. Barbone, Z. P. Sun, C. Galiotis, A. N. Grigorenko, G. Konstantatos, A. Kis, M. Katsnelson, L. Vandersypen, A. Loiseau, V. Morandi, D. Neumaier, E. Treossi, V. Pellegrini, M. Published on 25 March 2016. Downloaded by Drexel University on 25/03/2016 10:26:56.

Nanoscale

COMMUNICATION

- Polini, A. Tredicucci, G. M. Williams, B. H. Hong, J. H. Ahn, J. M. Kim, H. Zirath, B. J. van Wees, H. van der Zant, L. Occhipinti, A. Di Matteo, I. A. Kinloch, T. Seyller, E. Quesnel, X. L. Feng, K. Teo, N. Rupesinghe, P. Hakonen, S. R. T. Neil, Q. Tannock, T. Lofwandera and J. Kinaret, Nanoscale, 2015, 7, 4598-4810.
- M. Naguib, V. N. Mochalin, M. W. Barsoum and Y. Gogotsi, Advanced Materials, 2014, 26, 992-1005.
- 3. J.-C. Lei, X. Zhang and Z. Zhou, Frontiers of Physics, 2015, 10,
- M. Naguib and Y. Gogotsi, Accounts of Chemical Research, 2015, 48, 128-135.
- M. Naguib, O. Mashtalir, J. Carle, V. Presser, J. Lu, L. Hultman, Y. Gogotsi and M. W. Barsoum, ACS Nano, 2012, 6, 1322-1331.
- M. R. Lukatskaya, O. Mashtalir, C. E. Ren, Y. Dall'Agnese, P. Rozier, P. L. Taberna, M. Naguib, P. Simon, M. W. Barsoum and Y. Gogotsi, Science, 2013, 341, 1502-1505.
- M. Ghidiu, M. R. Lukatskaya, M.-Q. Zhao, Y. Gogotsi and M. W. Barsoum, Nature, 2014, 516, 78-81.
- X. Wang, S. Kajiyama, H. Iinuma, E. Hosono, S. Oro, I. Moriguchi, M. Okubo and A. Yamada, Nature Communications, 2015, 6, 6544.
- Y. W. Zhu, S. Murali, W. W. Cai, X. S. Li, J. W. Suk, J. R. Potts and R. S. Ruoff, Advanced Materials, 2010, 22, 5226-5226.
- 10. Y. Zhu, S. Murali, M. D. Stoller, K. J. Ganesh, W. Cai, P. J. Ferreira, A. Pirkle, R. M. Wallace, K. A. Cychosz, M. Thommes, D. Su, E. A. Stach and R. S. Ruoff, Science, 2011, 332, 1537-1541.
- 11. S. Malik, A. Vijayaraghavan, R. Erni, K. Ariga, I. Khalakhan and J. P. Hill, Nanoscale, 2010, 2, 2139-2143.
- 12. K. Zhang, L. Mao, L. L. Zhang, H. S. On Chan, X. S. Zhao and J. Wu, Journal of Materials Chemistry, 2011, 21, 7302-7307.
- 13. Y. Lin, K. A. Watson, J. W. Kim, D. W. Baggett, D. C. Working and J. W. Connell, Nanoscale, 2013, 5, 7814-7824.
- 14. Y. Xu, Z. Lin, X. Zhong, X. Huang, N. O. Weiss, Y. Huang and X. Duan, Nature Communications, 2014, 5, 4554.
- 15. O. Mashtalir, M. R. Lukatskaya, M. Q. Zhao, M. W. Barsoum and Y. Gogotsi, Advanced Materials, 2015, 27, 3501-3506.
- 16. Z. Ling, C. E. Ren, M. Q. Zhao, J. Yang, J. M. Giammarco, J. Qiu, M. W. Barsoum and Y. Gogotsi, Proceedings of the National Academy of Sciences of the United States of America 2014, **111**. 16676-16681.
- 17. Y. Gogotsi and P. Simon, *Science*, 2011, **334**, 917-918.
- 18. Y. Dall'Agnese, M. R. Lukatskaya, K. M. Cook, P.-L. Taberna, Y. Gogotsi and P. Simon, Electrochemistry Communications, 2014, 48. 118-122.
- 19. O. Mashtalir, M. Naguib, V. N. Mochalin, Y. Dall'Agnese, M. Heon, M. W. Barsoum and Y. Gogotsi, Nature Communication, 2013, 4, 1716.
- 20. Q. M. Peng, J. X. Guo, Q. R. Zhang, J. Y. Xiang, B. Z. Liu, A. G. Zhou, R. P. Liu and Y. J. Tian, Journal of the American Chemical Society, 2014, 136, 4113-4116.
- 21. Q. Zhang, J. Teng, G. Zou, Q. Peng, Q. Du, T. Jiao and J. Xiang, Nanoscale, 2016, DOI: 10.1039/C5NR09303A.
- 22. A. A. Levchenko, A. I. Kolesnikov, N. L. Ross, J. Boerio-Goates, B. F. Woodfield, G. Li and A. Navrotsky, The Journal of Physical Chemistry A, 2007, 111, 12584-12588.
- 23. E. C. Spencer, A. A. Levchenko, N. L. Ross, A. I. Kolesnikov, J. Boerio-Goates, B. F. Woodfield, A. Navrotsky and G. Li, The Journal of Physical Chemistry A, 2009, 113, 2796-2800.
- 24. C. T. Johnston, D. L. Bish, J. Eckert and L. A. Brown, The Journal of Physical Chemistry B, 2000, 104, 8080-8088.

- 25. N. Kumar, S. Neogi, P. R. C. Kent, A. V. Bandura, J. D. Kubicki, D. J. Wesolowski, D. Cole and J. O. Sofo, The വാഗനത്ത് എന്നിയുടിയോട Chemistry C, 2009, 113, 13732-13740.
- 26. J. Halim, K. M. Cook, M. Naguib, P. Eklund, Y. Gogotsi, J. Rosen and M. W. Barsoum, Applied Surface Science, 2016, 362, 406-417.
- 27. H.-W. Wang, M. J. DelloStritto, N. Kumar, A. I. Kolesnikov, P. R. C. Kent, J. D. Kubicki, D. J. Wesolowski and J. O. Sofo, The Journal of Physical Chemistry C, 2014, 118, 10805-10813.
- 28. T. Tipton, D. A. Stone, K. KuBulat and W. B. Person, The Journal of Physical Chemistry, 1989, 93, 2917-2927.
- 29. C. Raja, D. Dana, D. Luke and L. Zhenxian, Journal of Physics: Conference Series, 2014, 500, 052008.
- 30. G. Y. Yang, Y. C. Shi, X. D. Liu and A. S. Mujumdar, Drying Technology, 2007, 25, 675-680.
- 31. Z. Li, L. Wang, D. Sun, Y. Zhang, B. Liu, Q. Hu and A. Zhou, Materials Science and Engineering: B, 2014, 2015, 191, 33-40.
- 32. H. Ghassemi, W. Harlow, O. Mashtalir, M. Beidaghi, M. R. Lukatskaya, Y. Gogotsi and M. L. Taheri, Journal of Materials Chemistry A, 2014, 2, 14339-14343.
- 33. M. R. Lukatskaya, S.-M. Bak, X. Yu, X.-Q. Yang, M. W. Barsoum and Y. Gogotsi, Advanced Energy Materials, 2015, 5, 1500589.
- D. J. Jones and J. Roziere, in Proton Conductors: Solids, Membranes and Gels - Materials and Devices, ed. P. Colomban, Cambridge University Press, 1992, 18-37.